Light-front wavefunction dependence of quark recombination

Byungsik Hong*
Department of Physics, Korea University, Seoul 136-701, Korea

Chueng-Ryong Ji†
Department of Physics, North Carolina State University, Raleigh, North Carolina 27695, USA

Dong-Pil Min‡
Department of Physics and Astronomy, Seoul National University, Seoul 151-747, and Korea Research Foundation, Korea
(Received 6 October 2005; published 8 May 2006)

We present an extension of the recombination formalism to analyze the effects of variation of the hadron wavefunctions. The hadron spectra are sensitive to the shape of the wavefunctions. However, when we fit the wavefunction parameters to the physical observables, such as the average charge radius, the final spectra are very similar to one another. We discuss our numerical results in comparison with the published PHENIX and STAR data for the BNL Relativistic Heavy Ion Collider. In the hadron spectra, the recombination of thermal partons dominates at intermediate transverse momentum ($P_T = 2$–5 GeV), and the fragmentation dominates at high $P_T (>5$ GeV). The yield ratios and the nuclear modification factors for various hadron species are also estimated and compared with the experimental data. We present a new prediction for $\bar{p}/p$ and K^-/K^+ ratios, including the jet quenching effects on the fragmentation mechanism.

DOI: 10.1103/PhysRevC.73.054901 PACS number(s): 25.75.Dw, 12.39.−x

I. INTRODUCTION

Although no one doubts the existence of quarks and gluons, they have not yet been detected individually at zero temperature. The current vigorous efforts at the BNL Relativistic Heavy Ion Collider (RHIC) and the future plans of the CERN Large Hadron Collider (LHC) may reveal the temperature dependence of the confinement mechanism and the chrial symmetry restoration [1]. The high-energy nuclear collisions compress and heat the heavy nuclei so much that their individual protons and neutrons may overlap, and, in addition, a lot of pions may arise to ultimately create the quark-gluon plasma (QGP). The QGP may have existed ten millionths of a second after the Big Bang and may have created the primordial matter of the universe. The RHIC and the future LHC may yield the QGP in the laboratory. It has been reported that the four experiments at RHIC have already obtained distinguished results from the lower-energy heavy-ion collisions at CERN SPS [2–5]. The future LHC experiments (ALICE as well as CMS and ATLAS) would require theoretical predictions at a 30-fold energy increase from the RHIC.

Among many others, the effects of jet quenching and bulk hadronization may be regarded as important new results. Specifically, elliptic flow analysis revealed that the differential second-harmonic Fourier moment (v_2) of the azimuthal distribution with respect to the reaction plane had a remarkable saturation property in the intermediate transverse momentum (P_T) range between 2 and 6 GeV for all hadrons, including multistrange baryons. This saturation effect and eventual decrease of v_2 at high P_T have been qualitatively interpreted to be the results of partonic energy loss in an opaque parton system created by nuclear collisions [6,7]. Furthermore, the estimated v_2 parameter as a function of P_T is scaled by the number of constituent quarks of particles. Together with enhanced proton production in the intermediate P_T region, this agreement has been taken seriously as one piece of evidence for the quark recombination process and the presence of partonic collectivity at the early stage of a collision [8–13].

In this work we utilize the previous recombination formalism and extend it to analyze the light-front (LF) wavefunction dependence in the theoretical predictions from this formalism [8]. Typical forms of the LF wavefunctions, such as the Gaussian form and the power-law form, are applied to this extended formulation. The numerical results are contrasted to each other and compared with the available single invariant spectra from PHENIX and STAR for various mesons and baryons. We also discuss the production ratios of various hadrons, including $\bar{p}/p$ and K^-/K^+, in the fragmentation region. While we include the jet quenching effects as others do, we get a rather distinct results compared with the previous ones. For the high P_T regions, we get a dramatic suppression of the antiparticles $\bar{p}$ and K^- compared with the corresponding particles p and K^+, respectively.

The paper is organized as follows. In Sec. II we present the recombination formalism, which is extended from the previous one to explicitly include the intrinsic transverse momenta of the constituents inside the hadron. Rather than an extensive review of the previous formalism, we focus on what has been extended from the previous model. In Sec. III, we present the numerical results of the P_T spectra for various mesons and baryons to contrast the results between the Gaussian form and the power-law form. The results are compared with

*Electronic address: bhong@korea.ac.kr
†Electronic address: ji@ncsu.edu
‡Electronic address: dpmin@snu.ac.kr

the available experimental data from PHENIX and STAR Collaborations. We also discuss the production ratios of various hadrons and the nuclear modification factor $R_{\rm CP}$ in this section. Conclusions and discussions follow in Sec. IV.

II. FORMULATION

A. Recombination and light-front wavefunction dependence

The current data from the RHIC experiments seem to indicate two distinguished mechanisms of hadronization: (1) quark recombination for a rather low and intermediate P_T region and (2) quark fragmentation for a high P_T region. In this section we present an extension of the recombination formalism to analyze the effects from the variation of the hadron wavefunctions.

Introducing the density matrix $\hat{\rho}$ for the system of partons, the number of quark-antiquark states that one may interprete as mesons is given by

$$N_M = \sum_{ab} \int \frac{d^3P}{(2\pi)^3} \langle M; P|\hat{\rho}_{ab}|M; P\rangle, \tag{1}$$

where $|M; P\rangle$ is a meson state with momentum P and the sum is over all combinations of quantum numbers such as flavor, helicity, and color of the valence quarks that contribute to the given meson M. Inserting complete sets of coordinates and using the Wigner function formalism, one can derive the formula for the invariant spectrum of the meson M as follows [8]:

$$\begin{aligned} E\frac{d^3N_M}{dP^3} &= C_M \int_\Sigma \frac{d^3RP\cdot u(R)}{(2\pi)^3} \int \frac{d^3q}{(2\pi)^3} \\ &\quad \times w_a\left(R; \frac{P}{2} - q\right) \Phi_M^W(q) w_b\left(R; \frac{P}{2} + q\right) \\ &= C_M \int_\Sigma \frac{d^3RP\cdot u(R)}{(2\pi)^3} \int \frac{dx\,P^+ d^2\vec{k}_\perp}{(2\pi)^3} \\ &\quad \times w_a(R; xP^+, \vec{k}_\perp)\Phi_M(x, \vec{k}_\perp) \\ &\quad \times w_b(R; (1-x)P^+, -\vec{k}_\perp), \end{aligned} \tag{2}$$

where $\Phi_M^W(q) = \int d^3r \Phi_M^W(r, q)$ in the Wigner function formalism and $\Phi_M(x, \vec{k}_\perp) = |\psi_M(x, \vec{k}_\perp)|^2$ using the LF wavefunction of the meson $\psi_M(x, \vec{k}_\perp)$. Here, x and $\vec{k}_\perp$ are the momentum fraction and the respective intrinsic transverse momentum of each quark. Similarly, the invariant spectrum of the baryon B can be obtained as follows [8]:

$$\begin{aligned} E\frac{d^3N_B}{dP^3} &= C_B \int_\Sigma \frac{d^3RP\cdot u(R)}{(2\pi)^3} \int \frac{dx_1 P^+ d^2\vec{k}_{1\perp}}{(2\pi)^3} \\ &\quad \times \int \frac{dx_2 P^+ d^2\vec{k}_{2\perp}}{(2\pi)^3} \int \frac{dx_3 P^+ d^2\vec{k}_{3\perp}}{(2\pi)^3} \\ &\quad \times w_a(R; x_1P^+, \vec{k}_{1\perp}) w_b(R; x_2P^+, \vec{k}_{2\perp}) \\ &\quad \times w_c(R; x_3P^+, \vec{k}_{3\perp}) \Phi_B(x_1, x_2, x_3, \vec{k}_{1\perp}, \vec{k}_{2\perp}, \vec{k}_{3\perp}), \end{aligned} \tag{3}$$

where the constraints (or δ-functions) of $x_1 + x_2 + x_3 = 1$ and $\vec{k}_{1\perp} + \vec{k}_{2\perp} + \vec{k}_{3\perp} = 0$ are implied with appropriate phase factors.

The previous work by Fries and collaborators used a factorized ansatz for the LF wavefunction, for example [8],

$$\psi_M(x, \vec{k}_\perp) = \phi_M(x)\Omega(\vec{k}_\perp), \tag{4}$$

for mesons with a longitudinal distribution amplitude $\phi_M(x)$ and a transverse part $\Omega(\vec{k}_\perp)$. However, we note that such a factorization ansatz cannot be justified in free space, since the LF wavefunction depends on the LF invariant mass of the particle; e.g., for the meson $(m_a^2 + \vec{k}_\perp^2)/x + (m_b^2 + \vec{k}_\perp^2)/(1-x)$ (here the meson is composed of quark a and b), which cannot be factorized as Eq. (4). In general, the assumption of a wavefunction factorization such as Eq. (4) is not acceptable in free space because LF wavefunctions should be solutions of LF bound-state equations and the LF energy-momentum dispersion relation is rational, i.e. $k^- = ({k_\perp}^2 + m^2)/k^+$ for a particle with mass m. Both the LF kinetic energy (i.e., the LF invariant mass of the bound-state) and the LF kernel (or the inverse of the LF energy difference between the initial and intermediate states) involved in the LF bound-state equations are not factorizable owing to the rational energy-momentum dispersion relations. Thus the solutions of the LF bound-state equations cannot be factorizable, and we do not integrate over $\vec{k}_\perp$ in Eqs. (2) and (3) but leave $\vec{k}_\perp$ explicitly in the formulation. On the other hand, since it is not yet known whether the LF bound-state solution in free space is also applicable to the dynamical recombination process in quark matter without any modification, we note that the factorization ansatz used in Ref. [8] may be equally valuable as one of the model calculations in this work.

The usual parton spectrum at a given temperature is given by [8]

$$w_a(R; p) = \gamma_a e^{-p\cdot v(R)/T} e^{-\eta^2/2\Delta^2} f(\rho, \phi), \tag{5}$$

where ρ and ϕ are the radial and the azimuthal angle coordinates, respectively. In addition, $v(R)$ and η represent the velocity four-vector and the rapidity of the quark a, respectively. Here, $\gamma_a = \exp(\mu_a/T)$ is the fugacity factor for each quark species a for which we adopt the results from the statistical analysis for the hadron production at RHIC [14]: the chemical potential μ_a's are 9, 6.7, and -3.9 MeV for $a = u$ (or d), s, and c, respectively. Note that Ref. [14] gives the resulting chemical potentials for isospin, strangeness, and charm as well as the baryon chemical potential estimated by the statistical model at RHIC. Since statistical analysis of hadron production provides only chemical potentials of hadrons (not quarks), we obtained the quark fugacities by using the following formula for the fugacity of hadron i [15]:[1]

$$\Upsilon_i = \gamma_{I_3^i} \prod_a \gamma_a^{N_a^i}, \tag{6}$$

where N_a^i is the number of quark species a in hadron i. In Eq. (6) the fugacity $\gamma_{I_3^i}$ is close to 1, as the isospin chemical potential $\mu_{I_3^i}$ and the assumed freeze-out temperature T are -0.96 and 175 MeV, respectively [14]. We assume that the temperature T for hadronization occurs at 175 MeV. The lattice

[1]The quark fugacity γ_a in this paper means λ_a in Eq. (3) of Ref. [15] with the saturation factor 1.

QCD predicts that the phase transition occurs at $T = 175$ MeV at vanishing baryon chemical potential [16]. It should be reasonable that the temperature of the partonic phase is assumed to be the same as that of the phase transition. The space-time structure of the parton source in Eq. (5) is given by a transverse distribution $f(\rho, \phi)$ and a wide Gaussian rapidity distribution with width Δ. Also, one may assume $f(\rho, \phi) \approx \Theta(\rho_0 - \rho)$, especially for the analysis of the central collisions. With these assumptions, we find

$$\left.\frac{d^3N_M}{dP_T^2 dy}\right|_{y=0} = C_M M_T \frac{V}{(2\pi)^3} 2\gamma_a\gamma_b I_0\left[\frac{P_T \sinh\eta_T}{T}\right] \times \int_0^1 dx \int_0^\infty d^2\vec{k}_\perp |\psi_M(x,\vec{k}_\perp)|^2 k_M(x,\vec{k}_\perp, P_T), \tag{7}$$

where $V = \tau A_T$ (τ is the hadronization time and A_T is the transverse size) is the volume of the parton system and

$$k_M(x,\vec{k}_\perp, P_T) = K_1\left(\frac{\cosh\eta_T}{T}\left\{\sqrt{m_a^2 + (xP_T + \vec{k}_\perp)^2} + \sqrt{m_b^2 + [(1-x)P_T - \vec{k}_\perp]^2}\right\}\right). \tag{8}$$

We note that the particular combination of P_T and $\vec{k}_\perp$ for each constituent quark in Eq. (8) is consistent with the boost invariance of k_M in light-front dynamics. Extension to the baryon case is straightforward:

$$\left.\frac{d^3N_B}{dP_T^2 dy}\right|_{y=0} = C_B M_T \frac{V}{(2\pi)^3} 2\gamma_a\gamma_b\gamma_c I_0\left[\frac{P_T \sinh\eta_T}{T}\right] \times \int_0^1 dx_1 dx_2 \int_0^\infty d^2\vec{k}_{1\perp} d^2\vec{k}_{2\perp} |\psi_B(x_1, x_2, \times \vec{k}_{1\perp}, \vec{k}_{2\perp})|^2 k_B(x_1, x_2, \vec{k}_{1\perp}, \vec{k}_{2\perp}, P_T) \tag{9}$$

and

$$k_B(x_1, x_2, \vec{k}_{1\perp}, \vec{k}_{2\perp}, P_T) = K_1\left(\frac{\cosh\eta_T}{T}\left\{\sqrt{m_a^2 + (x_1P_T + \vec{k}_{1\perp})^2} + \sqrt{m_b^2 + (x_2P_T + \vec{k}_{2\perp})^2} + \sqrt{m_c^2 + [(1-x_1-x_2)P_T - (\vec{k}_{1\perp} + \vec{k}_{2\perp})]^2}\right\}\right). \tag{10}$$

In the following analysis, we take V as a free parameter to fit all invariant spectra of hadrons simultaneously for a given collision centrality.

With this extension, we can now explicitly include the effect from the intrinsic transverse momentum of each quark and vary the form of the LF wavefunction, such as the Gaussian form and the power-law form [17]. In this analysis we use the following typical LF wavefunctions for mesons and contrast the results between the two:

$$\psi_{\text{Gaussian}}(x,\vec{k}_\perp) = \exp\left[-\left(\frac{m_a^2 + \vec{k}_\perp^2}{x} + \frac{m_b^2 + \vec{k}_\perp^2}{1-x}\right)\Big/\beta^2\right], \tag{11}$$

and

$$\psi_{\text{Power-law}}(x,\vec{k}_\perp) = 1\Big/\left(\frac{m_a^2 + \vec{k}_\perp^2}{x} + \frac{m_b^2 + \vec{k}_\perp^2}{1-x} + \alpha^2\right)^n, \tag{12}$$

where β, α, and n are the parameters that can be fixed from the physical observables such as the size and the mass spectrum of the meson, etc. The extension of Eqs. (11) and (12) to baryons is rather straightforward:

$$\psi_{\text{Gaussian}}(x_1, x_2, \vec{k}_{1\perp}, \vec{k}_{2\perp}) = \exp\left[-\left(\frac{m_a^2+\vec{k}_{1\perp}^2}{x_1} + \frac{m_b^2+\vec{k}_{2\perp}^2}{x_2} + \frac{m_c^2 + (\vec{k}_{1\perp} + \vec{k}_{2\perp})^2}{1-x_1-x_2}\right)\Big/\beta^2\right] \tag{13}$$

and

$$\psi_{\text{Power-law}}(x_1, x_2, \vec{k}_{1\perp}, \vec{k}_{2\perp}) = 1\Big/\left[\frac{m_a^2 + \vec{k}_{1\perp}^2}{x_1} + \frac{m_b^2 + \vec{k}_{2\perp}^2}{x_2} + \frac{m_c^2 + (\vec{k}_{1\perp} + \vec{k}_{2\perp})^2}{1-x_1-x_2} + \alpha^2\right]^n. \tag{14}$$

In this calculation we used 260 MeV for the masses of u and d quarks and 460 MeV for the mass of the s quark. In a relativized quark model with chromodynamics, spectra of both mesons and baryons have been well analyzed. As shown in typical references ([18] for mesons and [19] for baryons), the potentials among constituents such as confinement, hyperfineness, spin-orbit, etc., work together to reproduce hadron spectra comparable with the experimental values. For instance, proton mass was predicted as 960 MeV, and the mass difference between nucleon and Δ was obtained as around 300 MeV, while the light quark mass was taken as 220 MeV. The same light quark mass was used to predict the meson spectra, which were in good overall agreement with the data. These support our light-front quark model calculations (see, e.g., Ref. [20]). Although we took the light quark mass 260 MeV as used in Ref. [8] for the present analysis, the essential predictions from a relativized quark model (or light-front quark model) remain intact.

Just to illustrate how typical LF wavefunctions look, we plot $\psi_{\text{Gaussian}}(x,\vec{k}_\perp)$ for different β^2 values in Fig. 1. As expected, the LF wavefunctions are symmetric around $x = 0.5$, if the masses of the constituent quark and antiquark are the same for pions. As β^2 increases, $\psi_{\text{Gaussian}}(x,\vec{k}_\perp)$ becomes broader in x as well as in $\vec{k}_\perp$. When the mass of the constituent quark and antiquark are not the same, like K and D, $\psi_{\text{Gaussian}}(x,\vec{k}_\perp)$'s are clearly skewed in x.

In order to constrain β, α, and n in Eqs. (11)–(14), the average values of $\vec{k}_\perp$ are fixed by the measured average charge radius square $\langle r^2\rangle$ of each hadron. If the experimental data for $\langle r^2\rangle$ are not available, we adopt those calculated by a relativistic quark model [21,22]. As an example, $\langle r^2\rangle = 0.44$ fm^2 for pions, and the corresponding β^2 is 0.825 GeV^2 for ψ_{Gaussian}. The average values of the charge radius square and the corresponding values of β^2 are summarized in

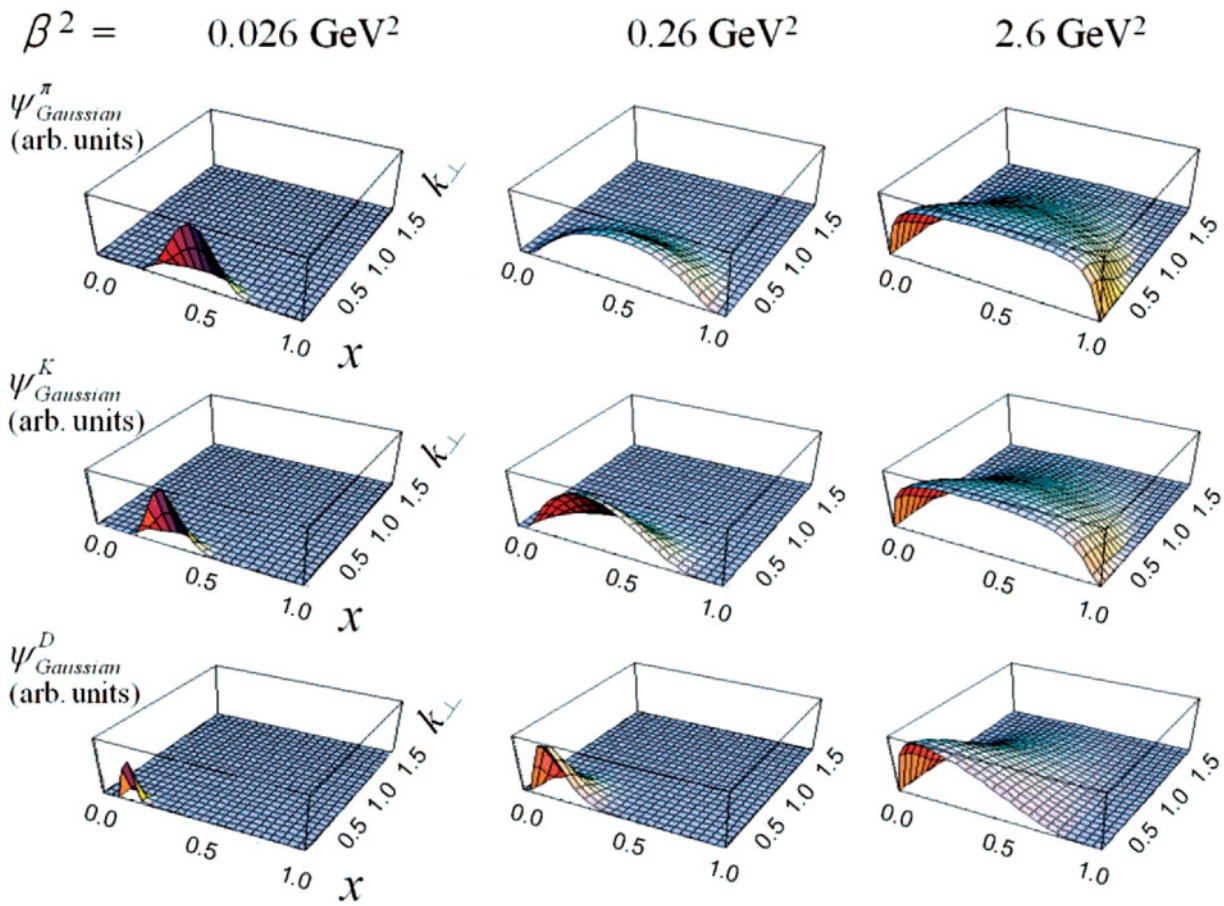

FIG. 1. (Color online) Shapes of the Gaussian wavefunctions as functions of x and $k_\perp$ for different β^2 (normalization is not performed in this figure). The top, middle, and bottom rows represent the wavefunctions for π, K, and D, respectively.

Table I. In addition, the deduced α^2 and n of $\psi_{\text{Power-law}}$ are 0.5 (1.53) GeV^2 and 2 (6), respectively, for pions (protons). The left two panels of Fig. 2 show the comparison of ψ_{Gaussian} and $\psi_{\text{Power-law}}$ of pions by using the adjusted wavefunction parameters. They demonstrate that the LF wavefunctions are very similar in shape when the parameters are determined by some physical observables such as the charge radii of hadrons. However, if we use some arbitrary values for those parameters, the shape of LF wavefunctions can be quite different, which is demonstrated in the lower right-hand panel of Fig. 2.

TABLE I. Deduced β^2 for the Gaussian LF wavefunctions used in this paper and the corresponding average charge radius square for various hadrons.

Particle	β^2 (GeV^2)	$\langle r^2 \rangle$ (fm^2)
π	0.825	0.44
K	1.06	0.34
ϕ	1.02	0.34
p	0.495	0.76
Λ	0.45	0.76
Ξ	0.47	0.76
Ω	0.48	0.76

The importance of the proper choice of the LF wavefunction parameters in the hadron spectra are explained in Fig. 3 for π's and protons. The invariant yields of the recombined hadrons are quite different for different sets of parameters. However, the hadron yields from the recombination process are quite similar for ψ_{Gaussian} and $\psi_{\text{Power-law}}$, once the wavefunction parameters are fixed by some physical observables (see solid versus dashed curves in Fig. 3.). In the following analysis, we use only the Gaussian wavefunction with proper β^2 for each hadron. For comparison, the wavefunctions used in Ref. [8] are also included in Fig. 3. The wavefunctions used in the present analysis (solid curves) are lower than the factorized wavefunctions used in Ref. [8], shown by dotted curves especially for the relatively low P_T region. Even on the logarithmic scale, the differences are as visible as the ones with arbitrary wavefunction parameters (dashed-dotted lines).

Since the essence of this work is to study the effect of the proper treatment of the LF wavefunctions for the recombination yields, we also compare the invariant spectra estimated by using full LF wavefunctions with those estimated by factorized wavefunctions. For the approximation that uses factorized wavefunctions for mesons, we tested $\psi_{\text{Gaussian}}(x, k_\perp)$ of Eq. (11) with $\langle \vec{k}_\perp^2 \rangle = 0.088$ GeV^2, multiplied by $\Omega(\vec{k}_\perp) = \exp(-\vec{k}_\perp^2/\beta^2)$ with $\beta^2 = 0.176\,\text{GeV}^2$, which gave us the right $\langle \vec{k}_\perp^2 \rangle$ value. The resulting invariant spectrum

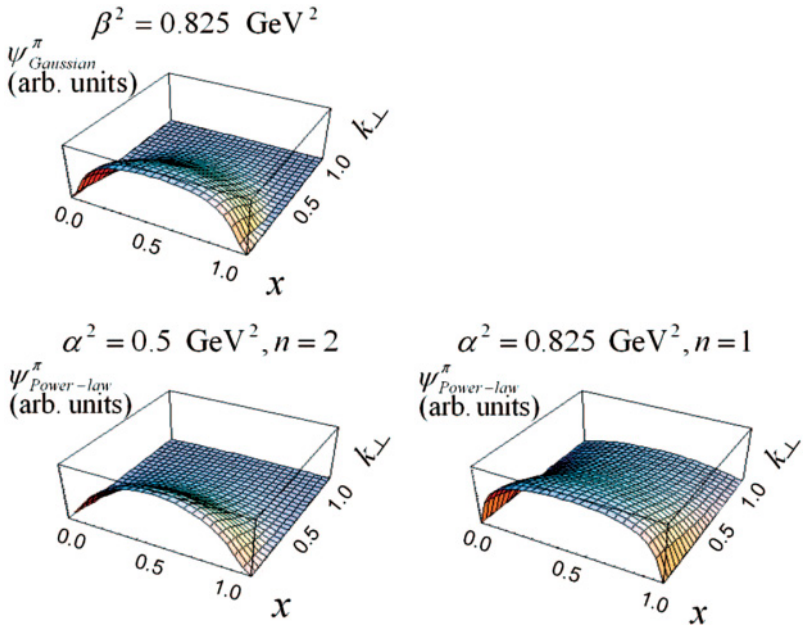

FIG. 2. (Color online) Comparison of the pion wavefunctions between the Gaussian form and the power-law form. The Gaussian wavefunction with $\beta^2 = 0.825$ GeV^2 (top) and the second-order power-law wavefunction with $\alpha^2 = 0.5$ GeV^2 (bottom left) are adjusted to the average charge radius of pions. But the first-order power-law wavefunction with $\alpha^2 = 0.825$ GeV^2 (bottom right) is not adjusted.

for the recombined π^+'s is very similar to the PL1 option in Fig. 3. Since it duplicates the result of the PL1 option, we do not display it explicitly in Fig. 3. However, this result indicates that the above factorized wavefunction may be as useful as

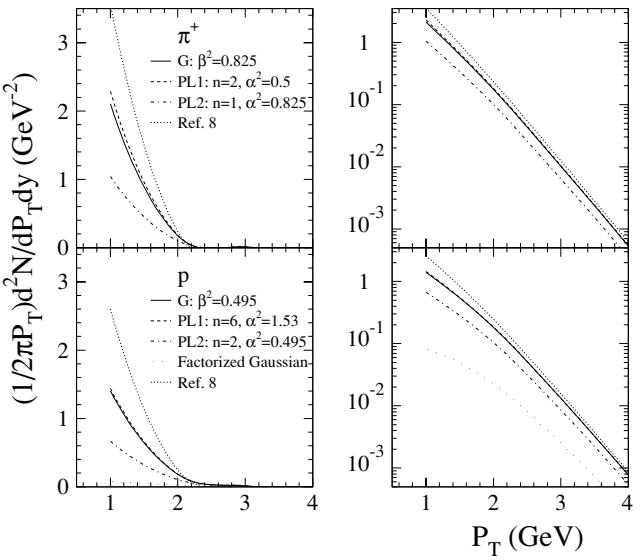

FIG. 3. Comparison of the invariant spectra of π^+ (top) and p (bottom) for the recombination process for various assumptions on the wavefunction parameters. Left-hand panels show the spectra on a linear scale to emphasize the difference in relatively low P_T regions, while the right-hand panels show them on log scale for comparison of the overall shapes. G represents the Gaussian wavefunction used in this paper. PL1 represents the power-law wavefunction whose parameters are adjusted by the known average charge radius, whereas PL2 represents the power-law wavefunction with arbitrary values for the parameters. The sparsely-dotted lines are calculated by a factorized Gaussian form of the LF wavefunctions with $\beta^2 = 0.495$ GeV^2 (see text for details). For comparison, the wavefunctions used in Ref. [8] are also plotted as the dotted curves.

the full LF wavefunctions developed in this paper for the phenomenological analysis of mesons, when the parameters are properly chosen.

Similarly, for baryons, we tested $\psi_{\rm Gaussian}(x_1, x_2, k_{1\perp}, k_{2\perp})$ of Eq. (13) with $\langle \vec{k}^2_{i\perp} \rangle = 0.0512$ GeV^2, multiplied by $\Omega(\vec{k}_\perp) = \exp[-(\vec{k}^2_{1\perp} + \vec{k}^2_{2\perp})/2\beta^2]$ with $\beta^2 = 0.495$ GeV^2. However, we could not find the proper β^2 value for the factorized wavefunction to get the correct $\langle k^2_\perp \rangle = 0.0512$ GeV^2, since the results were not at all stable (too large standard deviations). Thus, we instead varied the β^2 value over a wide range starting from 0.03 GeV^2 all the way to even above 1 GeV^2 and compared the resulting proton spectra. Results for β^2 below 0.03 GeV^2 could not be obtained owing to a numerical instability. The results for β^2 above 1 GeV^2 were about the same as the result of $\beta^2 = 1$ GeV^2 and were very stable as expected from the form of the above factorized wavefunction. Also, what we obtained for β^2 values from 0.03 GeV^2 to 1 GeV^2 was that the proton spectrum results were fairly insensitive to the β^2 value. The resulting invariant spectrum of the recombined protons are shown by the sparsely dotted curve (typically for $\beta^2 = 0.495$ GeV^2, but the result does not change much for other β^2 values) in the bottom panels of Fig. 3. The recombined proton yield of the factorized wavefunction is significantly lower than that of the nonfactorizable wavefunction. This comparison indicates that it may be more significant in the baryon case than in the meson case what form of the wavefunction is taken for prediction of the recombination process. Thus the proper treatment of the wavefunction seems particularly important for baryon production in the recombination process.

We note that there are also other approaches for the recombination process: Refs. [10] and [23] considered soft-hard recombination with a covariant coalescence model and fragmentation as a part of recombination, respectively. In addition, a recent work by Majumder, Wang, and Wang [24] discussed a derivation of the recombination model from a field theory description of jet fragmentation. They noted that an *ad hoc* formulation of the recombination model is valid only under

some strict conditions on the hadron wavefunction. Therefore, we note that the present development is not the first to consider the dependence of hadron wavefunctions in the recombination process.

B. Fragmentation and jet quenching

Inclusive hadron production by fragmentation at large momentum transfer can be described well by perturbative quantum chromodynamics (pQCD). In the framework of pQCD, the invariant yield of hadron h with momentum P is given by [8]

$$E\frac{d^3N_h^{\rm frag}}{dP^3} = \sum_a \int_0^1 \frac{dz}{z^2} D_{a\to h}(z) E_a \frac{d^3N_a^{\rm pert}}{dp_a^3}, \tag{15}$$

where the sum runs over all constituent quark species a in h. For the spectrum of parton a with momentum $p_a = P/z$ at midrapidity, we use the parametrization by pQCD:

$$E_a\frac{d^3N_a^{\rm pert}}{dp_a^3} = \left.\frac{d^2N_a^{\rm pert}}{2\pi p_{aT}dp_{aT}dy}\right|_{y=0} = \frac{K}{\pi}\frac{C}{(1+p_{aT}/B)^\kappa}, \tag{16}$$

where the parameters C, B, and κ are taken from leading-order pQCD calculations [25]. $K = 1.5$ is taken in order to consider higher-order corrections approximately [8]. Note that the number of partons in different collision centralities are obtained by scaling the number of binary nucleon-nucleon collisions ($N_{\rm coll}$) or, equivalently, by the nuclear thickness function (T_{AA}). The probability that parton a fragments into hadron h is taken into account by the fragmentation function

$$D_{a\to h}(z) = Nz^\gamma(1-z)^\delta, \tag{17}$$

where the numerical values of N, γ, and δ are taken from the parametrization by Kniehl, Kramer, and Pötter (Table 2 of Ref. [26] and the website http://www.desy.de/~poetter/kkp.f) for fragmentation of pions, kaons, protons, and antiprotons. We call this parametrization KKP parametrization. Λ fragmentation function is taken from the work by de Florian, Stratmann, and Vogelsang (Table I of Ref. [27]).

Finally, the energy loss of energetic partons (so called jet quenching), especially in central collisions, is considered with the following parametrization [28,29]:

$$\Delta p_T(b, p_T) = \epsilon(b)\sqrt{p_T}\frac{\langle L\rangle(b)}{R_A}, \tag{18}$$

where R_A is the radius of nucleus A, $\langle L\rangle(b)$ is the geometrical factor of the overlap zone of two nuclei, and $\epsilon(b)$ is the energy loss parameter of the hot medium with impact parameter b. The detailed functional forms of $\langle L\rangle(b)$ and $\epsilon(b)$ are the same as Ref. [8]:

$$\epsilon(b) = \epsilon_0\frac{1-\exp[-(2R_A-b)/R_A]}{1-\exp(-2)} \tag{19}$$

and

$$\langle L\rangle(b) = \frac{\sqrt{R_A^2-(b/2)^2}+(R_A-b/2)}{2}, \tag{20}$$

but, practically speaking, it is reasonable to assume that $\langle L\rangle(b) \simeq R_A$ and $\epsilon(b) \simeq \epsilon_0 = 0.82$ GeV$^{1/2}$ for the most central collisions as $b \to 0$.

III. RESULTS

A. Invariant spectra

Figure 4 shows the numerical results for the invariant spectra of various mesons at midrapidity for central Au + Au collisions at $\sqrt{s_{NN}} = 200$ GeV. In Fig. 4 we compare our calculations for the meson spectra with the published PHENIX and STAR data [30–34] up to $P_T = 10$ GeV in order to show the overall shapes, especially the transition regions near 5 GeV. The neutral pion spectrum was measured by PHENIX up to 10 GeV in P_T but lacks data in a low P_T region. In contrast, the charged pions were measured only at low P_T up to 3 GeV with high precision. However, the high P_T spectra of charged pions are expected to be very similar to those of neutral pions. For charged kaons, PHENIX measured up to 2 GeV, and STAR measured up to about 0.7 GeV in P_T. In general, the data by

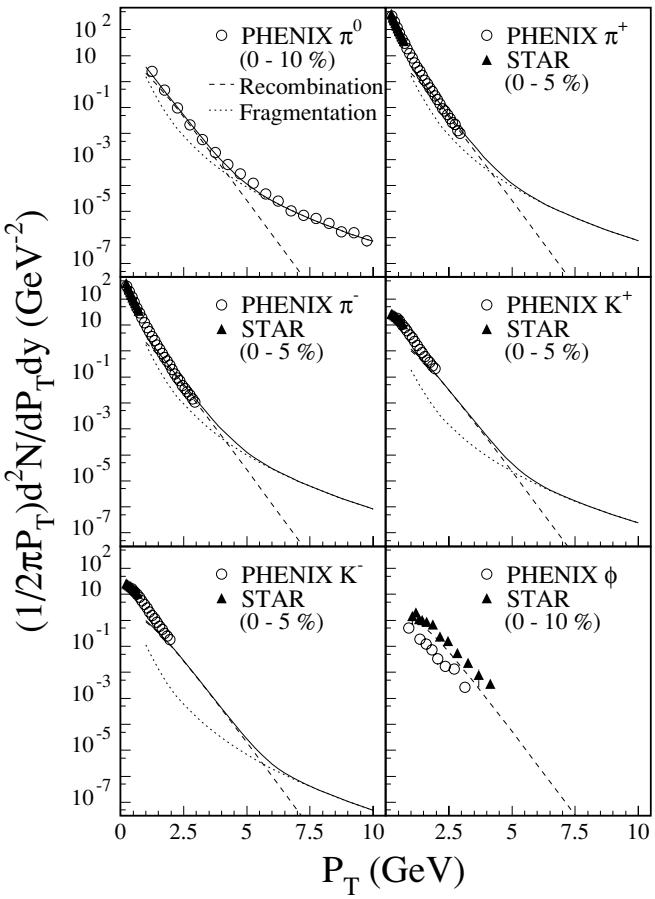

FIG. 4. Invariant spectra of mesons at midrapidity for central Au + Au collisions at $\sqrt{s_{NN}} = 200$ GeV. The dashed and dotted curves represent model calculations from recombination and fragmentation, respectively. The solid curves are the sum of the two contributions. The open circles are the data published by the PHENIX Collaboration [30–32], and the solid triangles are those by the STAR Collaboration [33,34].

PHENIX and STAR agree quite well in the overlapped phase space except for ϕ: the STAR data is about a factor of three larger than the PHENIX data.

In Fig. 4, the dashed and dotted curves represent the model calculations from recombination and fragmentation, respectively, and solid lines are the sum of the two contributions. In the π^0 spectra, the two distinguished P_T regions of hadron production are manifest. Although the transient P_T depends on the particle species, the recombination process is dominant between $\sim$2 and 5 GeV, and the fragmentation is dominant above 5 GeV. Our calculation is not expected to reproduce the hadron spectra below about 2 GeV in P_T. In such a very low P_T region the calculation underestimates the experimental data significantly, implying that other processes, like the transverse flow, the secondary decay of hadron resonances, and the binding energy effect, become important. Our calculation reproduces the measured meson P_T spectra larger than 2 GeV reasonable well, including the strange mesons. Note that we do not plot the fragmentation contribution for ϕ because of the lack of the fragmentation function.

Figure 5 shows the numerical results for the invariant spectra of baryons up to $P_T = 10$ GeV at midrapidity for central Au + Au collisions at $\sqrt{s_{NN}} = 200$ GeV. Figure 5 also compares the calculations with the published experimental data with the open circles for PHENIX [31,35] and the solid triangles for STAR [33,36,37]. The leftmost column of Fig. 5 is for protons and antiprotons; PHENIX and STAR measured up to about 5 and 1.2 GeV, respectively. Note that the P_T spectra for protons and antiprotons published by STAR [33] are about 40% higher than those by PHENIX [31]. This difference comes from the fact that the contributions from the Λ and Σ^0 decays are removed only for PHENIX. For a fair comparison between the two data sets, the p and $\bar{p}$ spectra by the STAR Collaboration are scaled by 0.6 in Fig. 5. After scaling down, the STAR spectra agree quite well with the PHENIX spectra in the overlapped phase space. The present model reproduces the measured proton and antiproton spectra reasonably well. The model also predicts that the transient P_T for baryons from recombination to fragmentation is somewhat higher than that for mesons.

In Fig. 5 the experimental invariant spectra of $\Lambda + \Sigma^0$, Ξ^-, Ω^-, and their antiparticles are for $\sqrt{s_{NN}} = 130$ GeV. But all model calculations are for $\sqrt{s_{NN}} = 200$ GeV, because all input parameters of the model calculations are available only for $\sqrt{s_{NN}} = 200$ GeV. Furthermore, owing to the lack of the fragmentation functions, we do not plot the fragmentation contribution for Ξ and Ω. Because of the difference in beam energy, the model overestimates the yields of $\Lambda + \Sigma^0$, Ξ^-, Ω^- and their antiparticles, and the discrepancy is larger for a larger number of strange quarks in a given baryon.

B. Yield ratios

One of the most interesting data from RHIC is the yield ratio of protons (or antiprotons) to pions at the intermediate

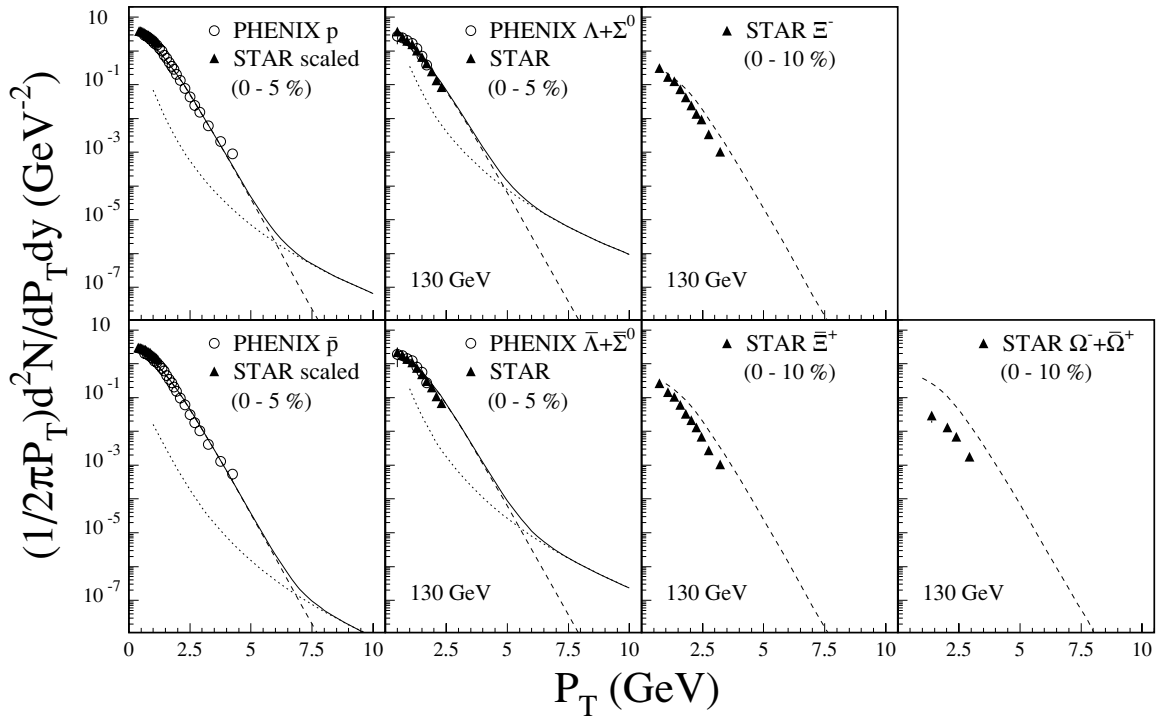

FIG. 5. Invariant spectra of baryons at midrapidity for central Au + Au collisions at $\sqrt{s_{NN}} = 200$ GeV. The dashed and dotted curves represent the model calculations from recombination and fragmentation, respectively. The solid curves are the sum of the two contributions. The open circles are the data published by the PHENIX Collaboration [31,35], whereas the solid triangles are those by the STAR Collaboration [33,36,37]. For a fair comparison between two sets of data, the published p and $\bar{p}$ spectra by the STAR Collaboration [33] are scaled by 0.6, which removes the contribution by the weak decays of Λ, Σ^0, and their antiparticles. Note that the experimental invariant spectra of hyperons are for $\sqrt{s_{NN}} = 130$ GeV, whereas all model calculations are for $\sqrt{s_{NN}} = 200$ GeV.

transverse momentum region ($2 < P_T < 5$ GeV) in central heavy-ion collisions. The p/π and $\bar{p}/\pi$ ratios rise steeply with P_T up to about 2.5 GeV but level off at about 1 and 0.7, respectively, in $2.5 < P_T < 5$ GeV for the most central 10% Au + Au collisions [31,38]. At $P_T > 2$ GeV, p/π and $\bar{p}/\pi$ for peripheral collisions are similar to those for elementary $p + p$ and e^+e^- collisions, and the ratios increase from peripheral to central collisions. Since the hydrodynamic model, which had been rather successful in describing the low P_T hadron spectra, could not explain the centrality dependence of limiting values, a recombination mechanism of hadronization at intermediate P_T was proposed as a possible resolution [8,10,23,39,40]. The recombination process naturally explains that the p/π and $\bar{p}/\pi$ ratios level off in $2 < P_T < 5$ GeV and fall sharply near $P_T \simeq 5$ GeV, where fragmentation overcomes recombination. Similar trends can also be found in the present calculation. The top row of Fig. 6 shows the results from our calculations for the p/π^0, $\bar{p}/\pi^0$, and $\bar{p}/p$ ratios in comparison with the published PHENIX data [31]. As P_T increases, the p/π^0 and $\bar{p}/\pi^0$ ratios rise, reach maximum values around 3 GeV, decrease sharply, and finally become constant at about 0.1 for $P_T > 6$ GeV. In addition, the $\bar{p}/p$ ratio is almost constant at about 0.9 for $P_T < 5$ GeV. However, it also decreases with P_T, and become almost constant at about 0.1 for $P_T > 7$ GeV, which is very different from the previous calculation by Fries *et al.* (the dashed line in Fig. 6) [8]. Although there is no dispute on KKP parametrizations [26] for gluon fragmentation, quark fragmentation is a problem because the KKP fragmentation functions are not fully flavor separated, and one has to make additional assumptions to separate contributions from different flavors. Incidentally, the recent STAR data on identified hadrons [41] reveal a poor job of the KKP fragmentation functions for p and $\bar{p}$ yields, possibly due to the lack of flavor separation. It seems that the sea quark contributions in $K^{\pm}$ and $\bar{p}/p$ are particularly problematic. For instance, as stated in Ref. [26], the d quark in $K^{\pm}$ does not behave as sealike, contrary to expectations. Thus even a slight difference in handling sea quark contributions could make a large difference in the predictions of ratios for K^-/K^+ and $\bar{p}/p$. Our results are based on maintaining the expected smallness of sea quark contributions consistently, not only in the pion case, but also in other hadron cases. Our low ratio for $P_T > 7$ GeV in $\bar{p}/p$ of Fig. 6 is consequently due to the dominance of valence contributions. It is a fact that incident heavy ions possess valence quarks, but not antiquarks. In other words, the charge conjugation symmetry is already broken in the RHIC environment because the initial nuclei carry only nucleons (not antinucleons). Since the baryon number (or, equivalently, the quark number) must be conserved throughout the reactions, more protons than antiprotons are expected in the fragmentation region.

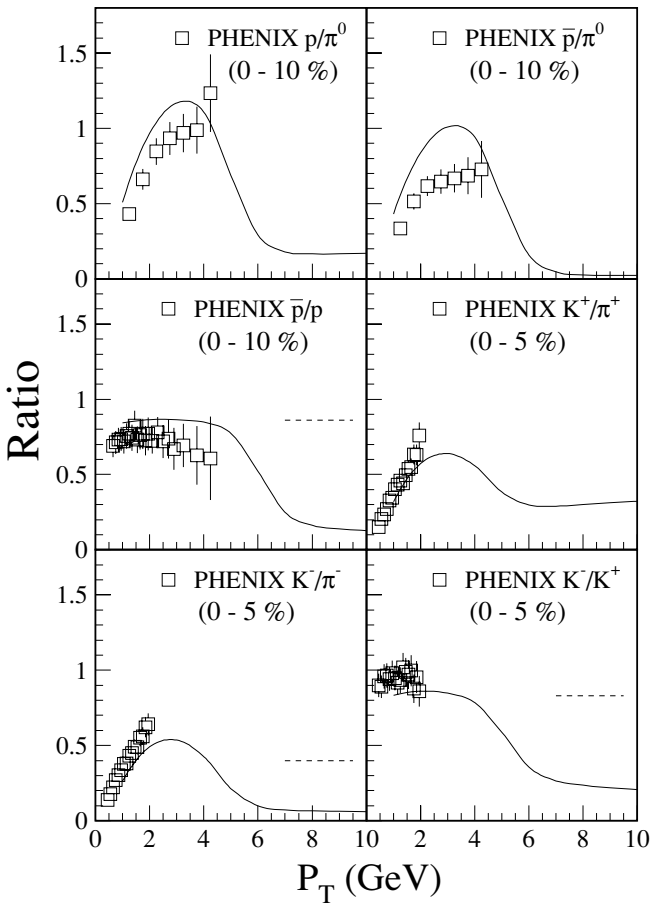

FIG. 6. Calculated hadron yield ratios (solid curves) as a function of P_T in comparison with the PHENIX data [31]. For comparison, we also show the model calculations by Fries *et al.*, in $\bar{p}/p$, K^-/π^-, and K^-/K^+, as dashed lines [8].

For more comparisons on the hadron yield ratios, the bottom row of Fig. 6 shows K^+/π^+, K^-/π^-, and K^-/K^+. Although the measured P_T range of $K^{\pm}$ is limited, the present estimates are in reasonable agreements with the data. The K^+/π^+ and K^-/π^- ratios increase with P_T and reach their maximum around $P_T = 3$ GeV. If P_T further increases, K^+/π^+ and K^-/π^- decrease and level off at some constants. The P_T dependence of the K^-/K^+ ratio is very similar to that of $\bar{p}/p$. Especially, we note that the present results on K^-/π^- and K^-/K^+ at high P_T region, where fragmentation is dominant, are quite different from the previous model calculations by Fries *et al.* [8]. As discussed above, even a slight difference in handling sea quark contributions could make a large difference in the predictions of ratios for K^-/K^+ as well as K^-/π^-. The forthcoming RHIC data at high P_T, e.g., the PHENIX data with newly installed aerogel detector, may help to further clarify the flavor separation issue in the KKP fragmentation functions [26].

C. Nuclear modification factors

Another important feature of the RHIC data can be identified in the nuclear modification factor $R_{\rm CP}$, which is defined by $N_{\rm coll}$ scaled central to peripheral yield ratios:

$$R_{\rm CP} = \frac{\text{Yield}^{\rm central} \big/ \langle N_{\rm coll}^{\rm central} \rangle}{\text{Yield}^{\rm peripheral} \big/ \langle N_{\rm coll}^{\rm peripheral} \rangle}. \tag{21}$$

The RHIC experiments observed that the $R_{\rm CP}$ parameters of various mesons in $P_T > 2$ GeV in central collisions were suppressed with respect to the $N_{\rm coll}$ scaled $p + p$ and peripheral collision data. Moreover, the suppression in the

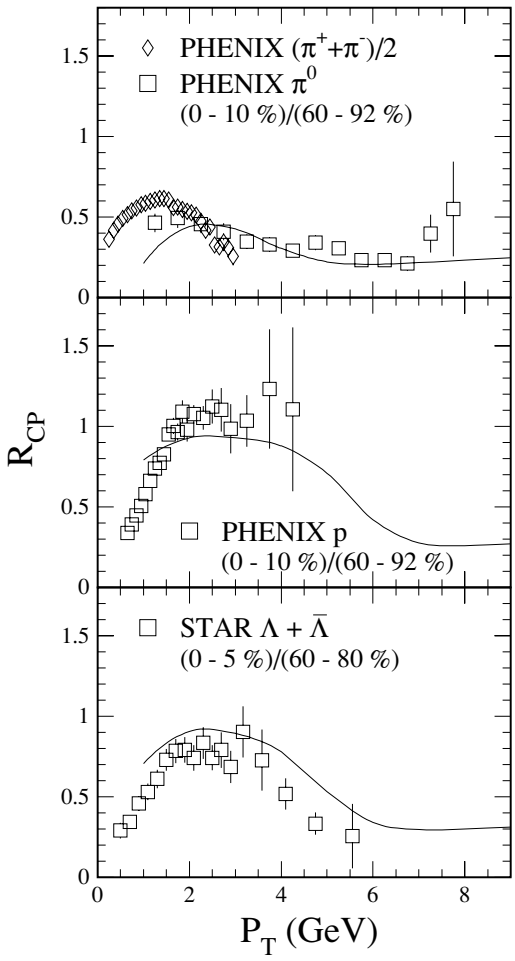

FIG. 7. Nuclear modification factors $R_{\rm CP}$ as a function of P_T for π, p, and $\Lambda + \bar{\Lambda}$. The solid curves are from the present calculation.

intermediate transverse momentum region ($2 < P_T < 4$ GeV) was only for mesons, not for baryons. The experimental $R_{\rm CP}$ parameter of protons in intermediate transverse momentum region is unity, which is completely consistent with $N_{\rm coll}$ scaling. The $R_{\rm CP}$ of Λ and $\bar{\Lambda}$ are also close to unity in an intermediate P_T region, but somewhat smaller than protons.

One possible explanation for the suppression of hadron yields at high P_T and the distinguished behavior of mesons and baryons in the intermediate P_T region is the combined effect of recombination and fragmentation. Figure 7 shows the estimated $R_{\rm CP}$ parameters of π, p, and $\Lambda + \bar{\Lambda}$ as a function of P_T. For pions, we plot charged and neutral pions together, as almost no difference is expected from the present model. In the present model calculation, we scaled the hadron yields due to fragmentation by a number of binary collisions. For the recombination part, the ratio of $V\prod_a \gamma_a$ in Eq. (7) for peripheral collisions to that in central collisions was assumed to be 40% of the participant ($N_{\rm part}$) ratio:

$$\frac{(V\prod_a \gamma_a)^{\rm peripheral}}{(V\prod_a \gamma_a)^{\rm central}} = c_1 \frac{N_{\rm part}^{\rm peripheral}}{N_{\rm part}^{\rm central}}, \tag{22}$$

where $c_1 = 0.4$ is fitted by the $R_{\rm CP}$ parameters of π, p, and $\Lambda + \bar{\Lambda}$, simultaneously, by fixing the temperature at 175 MeV, as it is almost independent of the collision centrality [42]. Since the quark fugacities are also almost constant except for the very peripheral collisions [42], the factor c_1 mostly reflects the effect of volume. As a result, the fact that $c < 1$ is understandable, as the flow velocity is larger for more central collisions. The agreement between the present calculations and the experimental data are reasonable for all considered hadron species.

IV. CONCLUSIONS

We have presented an extended formalism of the recombination model to analyze the effects from the variation of the hadron's light-front wavefunctions. Two different functional forms of the light-front wavefunction, which are the Gaussian form and the power-law form, are tested in detail. The hadron spectra are indeed sensitive to the shape of the wavefunctions. However, when we fit the wavefunction parameters to the physical observables, such as the average charge radius, the final spectra are very similar to one another. We discuss our numerical results in comparison with the published RHIC data, especially from the PHENIX and STAR Collaborations. In the hadron spectra the recombination of thermal partons dominates at the intermediate transverse momentum region between 2 and 5 GeV, and fragmentation dominates at high P_T, larger than 5 GeV. The yield ratios and the nuclear modification factors for various hadron species are also estimated. In general, the present model, which combines the recombination and fragmentation processes, is quite consistent with the experimental data. We have also discussed new predictions for $\bar{p}/p$ and K^-/K^+ ratios, including the jet quenching effects on the fragmentation mechanism.

ACKNOWLEDGMENTS

This work is supported in part by a grant from the U.S. Department of Energy (DE-FG02-96ER40947) and a brain-pool program from the KOFST (KOFST 042T-1-1) C.R.J. thanks the faculty and staff at the School of Physics at Seoul National University for the hospitality during the Sabbatical visit while this work was performed. We thank B. Mueller, R. Fries, S. Bass, and X.-N. Wang for useful discussions and information. The National Energy Research Scientific Computer Center is also acknowledged for the grant of supercomputing time.

[1] T. D. Lee, Nucl. Phys. **A750**, 1 (2005).
[2] I. Arsene *et al.* (BRAHMS Collaboration), Nucl. Phys. **A757**, 1 (2005).
[3] K. Adcox *et al.* (PHENIX Collaboration), Nucl. Phys. **A757**, 184 (2005).
[4] B. B. Back *et al.* (PHOBOS Collaboration), Nucl. Phys. **A757**, 28 (2005).
[5] J. Adams *et al.* (STAR Collaboration), Nucl. Phys. **A757**, 102 (2005).
[6] X. N. Wang, Phys. Rev. C **63**, 054902 (2001).

[7] M. Gyulassy, I. Vitev, and X. N. Wang, Phys. Rev. Lett. **86**, 2537 (2001).
[8] R. J. Fries, B. Müller, C. Nonaka, and S. A. Bass, Phys. Rev. C **68**, 044902 (2003); Phys. Rev. Lett. **90**, 202303 (2003).
[9] D. Molnár and S. A. Voloshin, Phys. Rev. Lett. **91**, 092301 (2003).
[10] V. Greco, C. M. Ko, and P. Levai, Phys. Rev. C **68**, 034904 (2003).
[11] T. S. Biro, P. Levai, and J. Zimanyi, Phys. Lett. **B347**, 6 (1995).
[12] P. Csizmadia and P. Levai, J. Phys. G **28**, 1997 (2002).
[13] B. Hong and J. Korean, Phys. Soc. **45**, L795 (2004).
[14] A. Andronic, P. Braun-Munzinger, K. Redlich, and J. Stachel, Phys. Lett. **B571**, 36 (2003).
[15] G. Torrieri and J. Rafelski, J. Phys. Conf. Ser. **5**, 246 (2005); arXiv:hep-ph/0409160.
[16] F. Karsch, Nucl. Phys. **A698**, 199 (2002).
[17] H.-M. Choi and C.-R. Ji, Phys. Rev. D **56**, 6010 (1997).
[18] S. Godfrey and N. Isgur, Phys. Rev. D **32**, 189 (1985).
[19] S. Capstick and N. Isgur, Phys. Rev. D **34**, 2809 (1986).
[20] H.-M. Choi and C.-R. Ji, Phys. Rev. D **59**, 074015 (1999).
[21] C.-R. Ji and S. R. Cotanch, Phys. Rev. D **41**, 2319 (1990).
[22] F. Schlumpf, Phys. Rev. D **50**, 6895 (1994).
[23] R. C. Hwa and C. B. Yang, Phys. Rev. C **70**, 024905 (2004).
[24] A. Majumder, E. Wang, and X.-N. Wang, Phys. Rev. C **73**, 044901 (2006).
[25] D. K. Srivastava, C. Gale, and R. J. Fries, Phys. Rev. C **67**, 034903 (2003).
[26] B. A. Kniehl, G. Kramer, and B. Pötter, Nucl. Phys. **B582**, 514 (2000).
[27] D. de Florian, M. Stratmann, and W. Vogelsang, Phys. Rev. D **57**, 5811 (1998).
[28] R. Baier, Y. L. Dokshitzer, A. H. Müller, and D. Schiff, J. High Energy Phys. 0109 (2001) 033.
[29] B. Müller, Phys. Rev. C **67**, 061901(R) (2003).
[30] S. S. Adler *et al*. (PHENIX Collaboration), Phys. Rev. Lett. **91**, 072301 (2003).
[31] S. S. Adler *et al*. (PHENIX Collaboration), Phys. Rev. C **69**, 034909 (2004).
[32] S. S. Adler *et al*. (PHENIX Collaboration), Phys. Rev. C **72**, 014903 (2005).
[33] J. Adams *et al*. (STAR Collaboration), Phys. Rev. Lett. **92**, 112301 (2004).
[34] J. Adams *et al*. (STAR Collaboration), Phys. Lett. **B612**, 181 (2005).
[35] K. Adcox *et al*. (PHENIX Collaboration), Phys. Rev. Lett. **89**, 092302 (2002).
[36] C. Adler *et al*. (STAR Collaboration), Phys. Rev. Lett. **89**, 092301 (2002).
[37] J. Adams *et al*. (STAR Collaboration), Phys. Rev. Lett. **92**, 182301 (2004).
[38] S. S. Adler *et al*. (PHENIX Collaboration), Phys. Rev. Lett. **91**, 172301 (2003).
[39] I. Vitev and M. Gyulassy, Phys. Rev. C **65**, 041902(R) (2002).
[40] R. C. Hwa and C. B. Yang, Phys. Rev. C **67**, 034902 (2003).
[41] J. Adams *et al*. (STAR Collaboration), arXiv:nucl-ex/0601033.
[42] F. Wang, Overview talk for the STAR Collaboration, presented at Quark Matter 2005 Conference, Budapest, Hungary, 4–9 August 2005, arXiv: nucl-ex/0510068; Nucl. Phys. A (2006) (in press).